PAPER

Atomic structure and Mott nature of the insulating charge density wave phase of 1T-TaS$_2$

To cite this article: V Petkov *et al* 2022 *J. Phys.: Condens. Matter* **34** 345401

View the article online for updates and enhancements.

Atomic structure and Mott nature of the insulating charge density wave phase of 1T-TaS$_2$

V Petkov[1],[*] ![ORCID]**, J E Peralta[1]** ![ORCID]**, B Aoun[2] and Y Ren[3],[4]**

[1] Department of Physics and Science of Advanced Materials Program, Central Michigan University, Mt. Pleasant, MI 48858, United States of America

[2] Fullrmc Inc., San Antonio, TX, 78255, United States of America

[3] X-ray Science Division, Advanced Photon Source, Argonne National Laboratory, Argonne, IL 60439, United States of America

[4] Department of Physics, City University of Hong Kong, Kowloon, Hong Kong, People's Republic of China

E-mail: petko1vg@cmich.edu

Abstract

Using x-ray pair distribution function (PDF) analysis and computer modeling, we explore structure models for the complex charge density wave (CDW) phases of layered 1T-TaS$_2$ that both well capture their atomic-level features and are amenable to electronic structure calculations. The models give the most probable position of constituent atoms in terms of 3D repetitive unit cells comprising a minimum number of Ta–S layers. Structure modeling results confirm the emergence of star-of-David (SD) like clusters of Ta atoms in the high-temperature incommensurate (IC) CDW phase and show that, contrary to the suggestions of recent studies, the low-temperature commensurate (C) CDW phase expands upon cooling thus reducing lattice strain. The C-CDW phase is also found to preserve the stacking sequence of Ta–S layers found in the room temperature, nearly commensurate (NC) CDW phase to a large extent. DFT based on the PDF refined model shows that bulk C-CDW 1T-TaS$_2$ also preserves the insulating state of individual layers of SD clusters, favoring the Mott physics description of the metal-to-insulator (NC-CDW to C-CDW) phase transition in 1T-TaS$_2$. Our work highlights the importance of using precise crystal structure models in determining the nature of electronic phases in complex materials.

Supplementary material for this article is available online

Keywords: charge density waves, atomic structure, total x-ray scattering

(Some figures may appear in colour only in the online journal)

1. Introduction

Among other transition metal dichalcogenides (TMDs), 1T-TaS$_2$ stands out with its remarkably rich pressure-temperature-light phase diagram, exhibiting several distinct charge density wave (CDW) phases and phase transitions. The material is built of layers of Ta–S trigonal prisms with a weak van-der-Waals bonding between the layers (figure 1(a)). Even at ambient pressure, a variety of phases appear upon cooling, including a metallic incommensurate (IC) CDW phase below 550 K, a metallic nearly commensurate (NC) CDW phase below 350 K and an insulating commensurate (C) CDW phase below 180 K. The metal–insulator (MI) transition between the

* Author to whom any correspondence should be addressed.
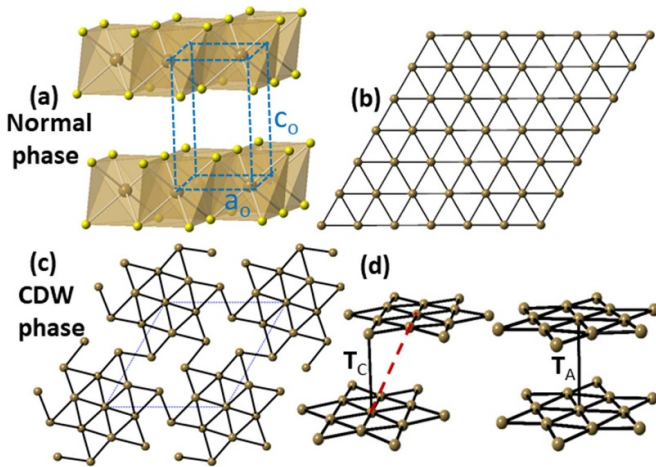
Figure 1. (a) Fragment from the crystal structure of 1T-TaS$_2$ comprising layers of Ta (brown)–S (yellow) prisms. In undistorted 1T-TaS$_2$ (b), Ta atoms form perfect hexagonal planes. In the C-CDW phase of 1T-TaS$_2$, Ta atoms form SDs organized in a $\sqrt{13}a_0 \times \sqrt{13}a_0$ superstructure, whose projection down the c axis is shown in (c). Possible stacking sequences of layers of SDs in the C-CDW phase are shown in (d). Here T_A and T_C are stacking vectors corresponding to the case of SDs from adjacent layers being positioned on top of each other and shifted by a lattice translation 2**a**, respectively. Broken red line connects Ta atoms at the center of SDs from adjacent Ta–S layers in the case of T_C-type stacking.

NC-CDW and C-CDW phases is first order and, upon cooling, accompanied by a large jump in resistivity that can be reversed by an application of intense electrical current or light pulse [1–5]. In the CDW phases, Ta atoms assemble in characteristic star-of-David (SD)-shaped clusters, which form an increasingly ordered 3D superstructure with decreasing temperature (figure 1(c)). For comparison, Ta atoms in normal metallic 1T-TaS$_2$ occupy the vertices of a perfect hexagonal lattice (figure 1(b)).

Regardless of the extensive research effort over nearly four decades, there is still an ongoing debate about the nature of the insulating C-CDW phase. Generally, it has been regarded as a Mott insulator phase, where thirteen 5d electrons, one from each Ta atom in an SD, form six covalent bonds and a half-filled band that does not exhibit a metallic but unusual insulating character due to strong electron-electron interactions. However, recently, this interpretation has been challenged by several studies, which attribute the insulating behavior to the emergence of a particular stacking order of Ta–S layers below 180 K, rendering the C-CDW phase a trivial band insulator (figure 1(d)) [6–8]. To distinguish between the two interpretations, precise knowledge of the atomic structure of CDW phases of 1T-TaS$_2$ is needed. At present, this knowledge is incomplete because the phases have been largely studied by traditional crystallographic techniques that largely ignore the presence of significant diffuse scattering in their diffraction patterns arising from the presence of significant lattice distortions inherent to CDWs. Moreover, structure data determined by single-crystal diffraction experiments are presented in supercells that are not necessarily amenable to electronic

properties calculation and interpretation. Here we use x-ray pair distribution function (PDF) analysis to investigate the atomic-level evolution of CDWs in 1T-TaS$_2$ over a broad temperature range, including the IC- to NC- and NC- to C-CDW phase transitions. We explore 3D structure models for the CDW phases that comprise a minimum number of Ta–S layers and refine them against the experimental PDF data. The models give the most probable position of constituent Ta and S atoms in terms of small-size, repetitive unit cells, allowing a convenient derivation of structural characteristics such as bond distances, degree of structural coherence and interlayer separation that are important for understanding the nature of CDW transitions, observed hysteresis effects and so-called 'hidden' CDW phases [1, 2]. Also, the PDF-refined models provide a sound basis for electronic structure calculations, allowing us to probe the character of the insulating C-CDW phase.

2. Synchrotron x-ray experiment, derivation of atomic PDFs and Rietveld analysis of x-ray diffraction (XRD) data

A high-quality 1T-TaS$_2$ sample was provided by 2DSemiconductors [9]. High-energy XRD data were collected on the beamline 11-ID-C at the Advanced Photon Source at the Argonne National Laboratory using x-rays with energy of 105.5 keV (wavelength $\lambda = 0.1173$ Å). The instrument was calibrated using Si powder National Institute of Standarts and Technology (NIST) standard. The sample was sealed in a glass capillary and measured in transmission mode. Scattered intensities were collected with a 2D amorphous Si detector. Oxford Cryostream 700+ device was used to control the temperature of the sample. Data were taken upon cooling the sample from 400 K to 140 K and subsequently warming it up to 250 K. Two sets of XRD patterns were collected at each temperature. One of the patterns was collected with the detector positioned 1000 mm away from the sample to achieve high-q resolution needed for Rietveld analysis, where the wave vector q is defined as $q = 4\pi\sin(\theta)/\lambda$ and θ is the Bragg angle. Exemplary XRD patterns collected at different temperatures are shown in figure 2(a). The patterns exhibit sharp Bragg peaks and weak satellite reflections that change little and significantly with temperature, respectively. As shown in previous studies, the former reflect the characteristic structure of 1T-TaS$_2$ built of layers of Ta–S trigonal prisms (figure 1(a)), whereas the latter signal the appearance of an increasingly ordered array of SDs (figure 1(c)) with diminishing temperature [1, 10, 11]. The other pattern was collected with the detector positioned 300 mm away from the sample to reach q values as high as 30 Å^{-1}. This pattern was used to obtain atomic PDFs with high real-space resolution, as described in supplemental material [12]. All experimental atomic PDFs obtained in this work are shown in figure 2(b). Comparison between the experimental and computed data sets in figure 2(c) indicates that atomic PDFs are sensitive to atomic correlations involving Ta atoms from emerging SDs in 1T-TaS$_2$.
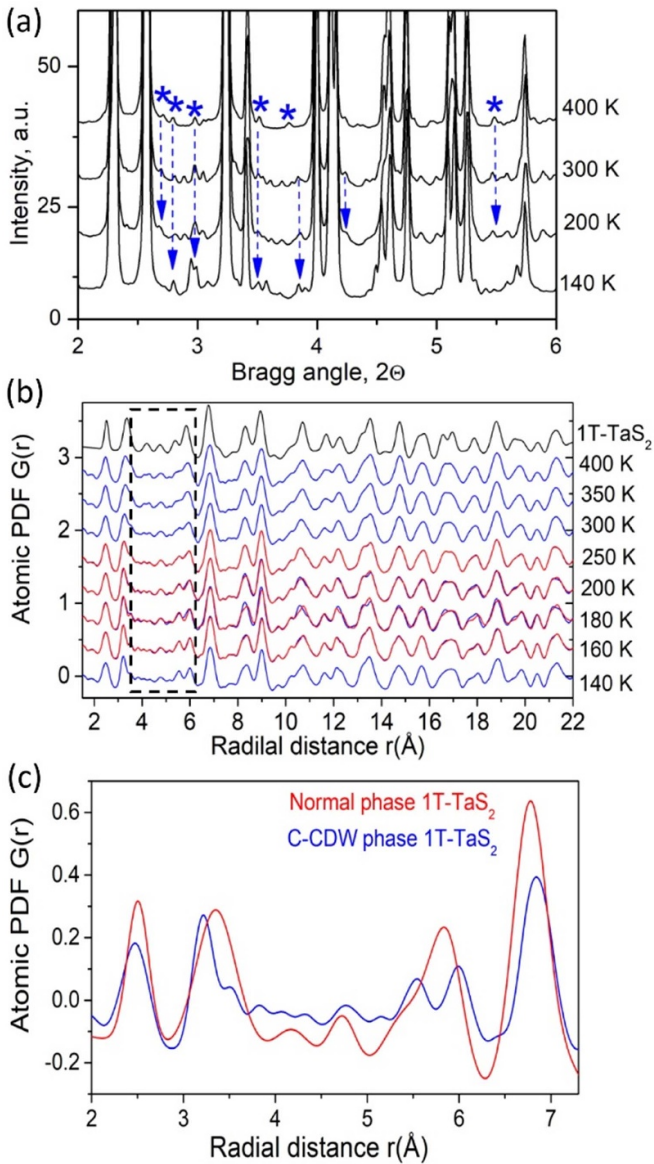
Figure 2. (a) High-energy XRD patterns for CDW phases of 1T-TaS$_2$ collected at different temperature upon cooling the sample. Satellite reflections in the XRD pattern obtained at 400 K are marked with blue stars. Vertical blue arrows highlight their evolution with temperature. (b) Experimental atomic PDFs obtained from XRD patterns collected upon cooling (blue line) and warming (red line) the sample. The PDFs exhibit hysteresis effects in the temperature range from 160 K to 200 K, i.e. appear different when obtained at the same temperature once upon cooling and a second time upon warming the sample. Computed PDF for normal (S.G. P-3m1) 1T-TaS$_2$ is also shown (black line) for comparison. It is different from the experimental PDFs, in particular in the range of r-values from 3 Å to 6 Å (outlined with a broken line), where near neighbor Ta–Ta distances appears as PDF peaks. This is because Ta atoms in normal 1T-TaS$_2$ do not while those in the CDW phases of 1T-TaS$_2$ cluster, as shown in figure 1. The difference between PDFs of normal and C-CDW phases is highlighted in (c).

Experimental high-*q* resolution XRD patterns were subjected to Rietveld analysis based on the hexagonal (S.G. P-3m1) structure of normal 1T-TaS$_2$. The computations were done with the help of software GSAS II [13]. Exemplary results
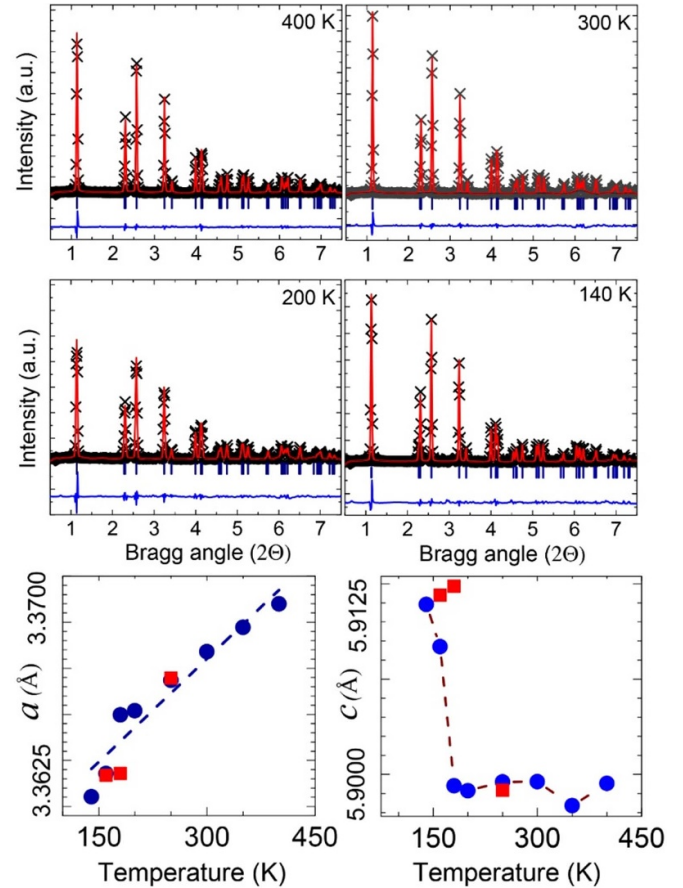
Figure 3. (First and second row) Exemplary Rietveld fits (red line) to high-energy XRD patterns (symbols) for 1T-TaS$_2$ collected at different temperatures. The fits are based on the hexagonal (S.G. P-3m1) structure characteristic to its normal metallic phase. The residual difference (blue line) is shifted by subtracting a constant. Good quality fits ($R_{wp} \sim 6\%$–8%) are achieved without applying corrections for preferred orientation, indicating that, thanks to the careful sample preparation and 2D geometry of the x-ray detector used, possible texture effects in the XRD patters are largely eliminated. (Third row) Hexagonal lattice parameters *a* and *c* for 1T-TaS$_2$ as a function of temperature resulted from Rietveld fits to XRD data measured upon cooling (blue dots) and warming (red squares). Data for the lattice parameters show a clear discontinuity at about 180 K, where the NC- to C-CDW phase transition takes place.

are shown in figure 3. As can be seen in the figure, sharp Bragg peaks in the XRD patterns are reproduced very well by the model, indicating that the material is single phase. In line with prior findings [1], the refined lattice parameters show discontinuities at 350 K and 180 K, reflecting the emergence of NC-CDW and C-CDW phases upon cooling, respectively. The presence of SD-like clusters of Ta atoms already at 400 K and the emergence of a superstructure of well-defined SDs at low temperature, however, are not immediately obvious from traditional Rietveld analysis of XRD patterns. On the other hand, atomic PDF analysis, which considers the Fourier transform of XRD data in real space without *a priory* assumption for the lattice symmetry, has proven very successful in revealing well both the long-range crystal structure and deviations from it, including emerging CDWs in low-dimensional

systems [14, 15]. As shown below, it is also very sensitive to the 3D arrangement of the SDs in 1T-TaS$_2$.

3. PDF-guided modeling of CDW phases in 1T-TaS$_2$

3.1. Scientific problem and approach to finding a solution to it

Above 350 K, satellite reflections in the XRD patterns are relatively weak and diffuse (see the asterisks in figure 2(a)) because the IC-CDW that causes them lacks translational periodicity. As such, it is impossible to be described by a unit cell that is periodic in 3D. Below 350 K, the satellite reflections increasingly become sharp with decreasing temperature, signaling the emergence of the NC-CDW phase. Similarly to the IC-CDW phase, it is difficult to be described by a unit cell periodic in 3D. Both the IC-CDW and NC-CDW phases, however, could be described in superspace using a unit cell of the 'basic' undistorted structure and modulation functions giving the displacements of Ta atoms from their positions in that structure [11, 16]. The superspace approach reproduces well both the Bragg peaks and satellite reflections but it does not lend itself to electronic structure calculations, which require 3D periodicity, and are necessary to understand physical properties of IC-CDW and NC-CDW phases in good detail. Below 180 K, the CDW appears commensurate with the underlying crystal lattice and the satellite reflections can be described in various lattices [17–19], whose base is shown in figure 1(d). However, positions of atoms in the typically very large unit cells of these lattices are not well known and/or the lattices appear non-periodic in a direction perpendicular to the layers of SDs, leading to ambiguities in selecting a proper 3D periodic unit cell for computing the electronic properties and interpreting the nature of emerged insulating state. To resolve the ambiguities, we generated 3D periodic, small unit size models for the three CDW phases of 1T-TaS$_2$ using published data for commensurate approximations to the phases and isostructural 1T-TaSe$_2$ [17, 20]. The models were refined against the respective experimental PDFs, which, by definition, give the probability of finding an atom at a certain distance from a given atom. Thus, these models give the most probable positions of atoms in the phases, allowing us to explore atomic-level features relevant to their structure type and electronic properties on a realistic basis. The computations were done with the help of the software PDFgui [21].

3.2. Solution implementation

3.2.1. IC-CDW phase (350 K–550 K).
A commensurate, i.e. 3D periodic approximation to the atomic structure of NC-CDW phase of 1T-TaS$_2$ has been proposed in [16] using single crystal data, including 836 satellite reflections. The approximation features a $a = b = \sqrt{13}a_o$ and $c = 3c_o$ hexagonal unit cell (S. G. P-3) comprising a stack of three Ta–S layers, where a_o and c_o are the lattice parameters of the undistorted lattice and Ta atoms are displaced from their positions in that lattice in a manner resembling the formation of SDs. We used it to create an initial model for the IC-CDW phase, the rationale being that the NC-CDW and

IC-CDW phase ought to share common structural features because diffuse satellite reflections in the XRD pattern for the latter appear 'precursors' of the better-defined reflections observed in the XRD pattern for the former. The initial model was successfully refined against the atomic PDF data measured at 400 K, which take into account observed Bragg peaks, superlattice reflections and diffuse scattering arising from the emergence of SD-like clusters in IC-CDW 1T-TaS$_2$. As can be seen in figures 4(a) and (b), the PDF-refined structure model reproduces the experimental PDF data up to 100 Å, where the experimental data decay to zero due to the finite q-space resolution of the 2D detector used. The refined lattice parameters and atomic positions are given as supplemental material [12]. The success of the refinement indicates that the 1T-TaS$_2$ sample studied by us exhibits structural features typical for the CDW phases of 1T-TaS$_2$ and atomic PDFs are capable of capturing these features.

3.2.2. C-CDW phase (below 180 K).
Several model structures for the C-CDW phase of 1T-TaS$_2$ have been proposed [17], including a structure based on a T_c stacking sequence alone (see figure 1(d)). Such a structure has been found successful in describing the C-CDW phase of 1T-TaSe$_2$ using a periodic unit cell with parameters $a = b = \sqrt{13}a_o$ and $c = 13c_o$ that comprises 13 Ta–S layers, i.e. a very large number of atoms. We constructed a minimum size model approximation to the structure of the C-CDW phase of 1T-TaS$_2$ featuring a single layer primitive unit cell (S.G. P-1) using a similar approximation to the structure of the C-CDW phase of 1T-TaSe$_2$. It was successfully refined against the experimental PDF data for 1T-TaS$_2$ collected at 140 K that take into account Bragg peaks, superlattice reflections and diffuse scattering arising from lattice distortions due to the formations of an ordered array of well-defined SDs and likely orientational disorder of the layers of SDs. As can be seen in figures 4(c) and (d), the refined model reproduces very well the experimental PDF data both at low and high-*r* distances extending up to 100 Å. The refined atomic positions and lattice parameters are given as supplemental material [12].

Another frequently considered model structure for the C-CDW phase of 1T-TaS$_2$ features two layers stacked on top of each other (T_A stacking vector in figure 1(d)) where the so-formed bilayers are further stacked by a random choice of symmetry equivalent vectors of the T_c type shown in figure 1(d) [17–19]. Because the disordered stacking of bilayers does not obey translational symmetry in the direction perpendicular to the *c* axis of the unit cell, an approximation to the model is often employed where the stacking of the bilayers follows a fixed T_c vector [18, 22]. Within this model picture, on average, half of the stacking vectors in the C-CDW phase would appear as T_A vectors and the other half would appear as T_c vectors, where T_A and T_c vectors alternate along the *c* direction of the crystal lattice. A model approximation to the structure of C-CDW phase featuring a T_A-type stacking sequence alone was constructed, tested and refined against experimental PDF data. It was, however, and found to perform worse in comparison to the model featuring a T_C-type stacking
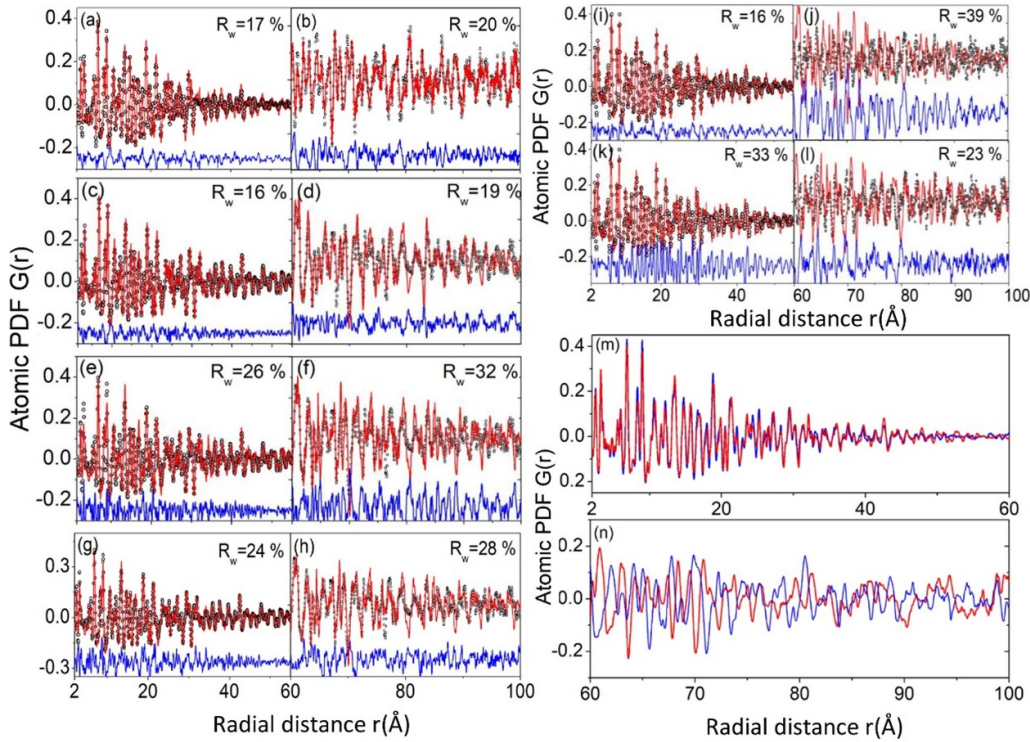
Figure 4. Structure model fits (red line) to experimental atomic PDFs (symbols) for CDW phases of 1T-TaS$_2$. The residual difference (blue line) is shifted by a constant for clarity. Fits in (a) and (b) are against PDF data obtained at 400 K (IC-CDW phase) and feature a commensurate model approximation (S.G. P-3) that fits the experimental data well over a wide range of *r*-values. Fits in (c)–(h) are against PDF data for the C-CDW phase obtained at 140 K. A model featuring a T_c stacking sequence (c), (d) outperforms models featuring a T_A sequence alone (e), (f) and a mixture of T_A and T_c stacking sequences (g), (h). Fits in (i)–(l) are against PDF data for the NC-CDW phase obtained at 250 K. Only the fit in (i), featuring a C-CDW type structure, and fit in (l), featuring an IC-CDW type structure, approximate the experimental data to an acceptable level. (m) Low- and (n) high-*r* part of PDF data obtained at 180 K upon cooling (blue) and a subsequent warming (red) the sample. The PDF data sets in (n) do not while those in (m) agree well with each other, indicating the presence of significant thermal hysteresis effects largely involving longer-range atomic correlations in NC-CDW 1T-TaS$_2$. Higher-r PDF data (b), (d), (f), (h), (j), (l) are multiplied by a factor of four for clarity.

sequence alone (figures 4(e) and (f)). The result is in line with the findings of density functional theory (DFT) studies [7] indicating that the latter is more stable energetically in comparison to the former. A model approximation featuring a mixture of T_A- and T_C-type stacking sequences was also found to perform worse in comparison to that featuring a T_C-type stacking sequence alone (figures 4(g) and (h)). The result is in line with recent scannig tunneling microscopy (STM) and transmission electron microscopy (TEM) studies indicating that Ta atoms in Ta–S layers constituting the C-CDW phase are well ordered along the out-of-plane direction, i.e. that the C-CDW phase is unlikely not exhibit a large variety of layer stacking orders [6, 23–25]. Thus, according results of PDF analysis, a model featuring a T_c-type stacking sequence appeared a better approximation to the structure of C-CDW phase in comparison to other frequently considered approximations based on a T_A-type stacking sequence.

3.2.3. NC-CDW phase. Considering that the NC-CDW phase is a precursor of the C-CDW phase, the PDF refined model for the latter was used to produce an initial model for the structure of the former. The model was tested and refined

against the PDF data for the NC-CDW phase obtained at 300 K. As shown in figure 4(i), the refined model reproduces the experimental data at distances shorter than 60 Å in very good detail. The PDF-refined atomic positions and lattice parameters are given as supplemental material [12]. It, however, fails to fit well the PDF data at high-*r* values (figure 4(j)). That part of the PDF data is well fit (see figure 4(l)) by the model approximation used to describe the IC-CDW phase, which is a precursor of the NC-CDW phase. The latter model, however, performs poorly at low-*r* distances (see figure 4(k)). Similarly to the findings of prior studies [8, 10, 23, 24, 26], the result indicates that the NC-CDW phase is discomensurate in a sense that it is built of approximately 60 Å in size lattice domains exhibiting the structure of C-CDW phase, where the SDs are well defined and Ta–S layers are largely stacked in a T_C-type sequence, that are embedded in a matrix exhibiting the lattice structure of the IC-CDW phase, where the SDs are less well defined and, as discussed below, Ta–S layers are more densely stacked in comparison to those in the domains.

Experimental PDFs obtained at 180 K once upon cooling the sample down to 140 K and a second time upon subsequently warming it to 180 K are shown in figures 3(m) and (n). The PDFs agree very well at low-r
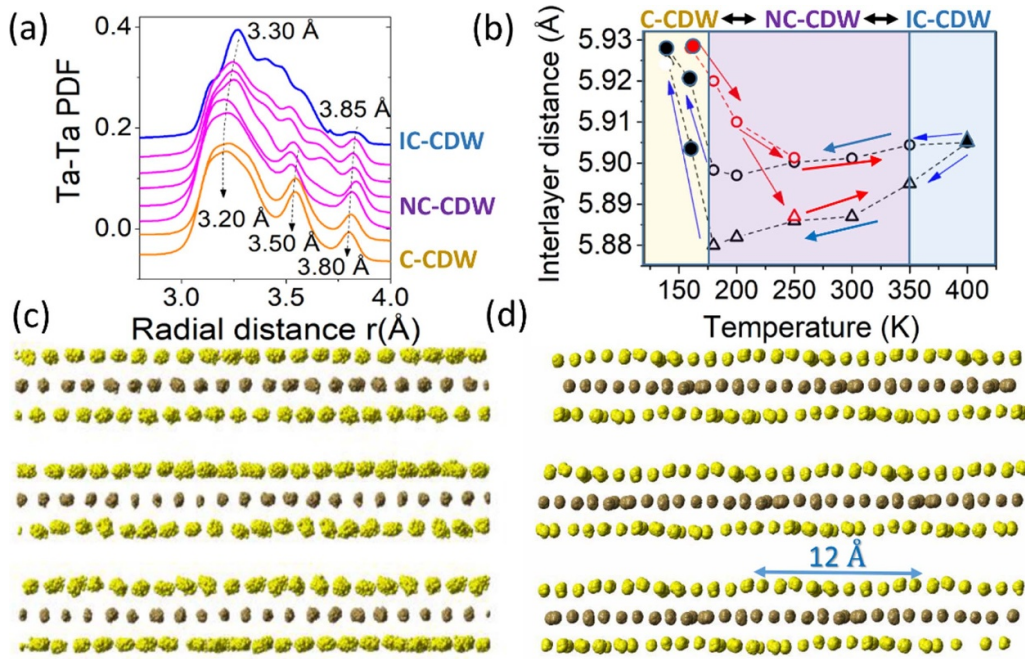
Figure 5. (a) Distribution of near-neighbor Ta–Ta distances extracted from PDF-refined structure models. The distances show a broad distribution already at 400 K due to local Ta clustering effects. The distribution develops distinct peaks with decreasing temperature (follow the dotted arrows), reflecting the emergence of well-defined SDs. (b) Evolution of the interlayer distance in the IC-CDW (light blue area), NC-CDW (light magenta area) and C-CDW (light green area) phases of 1T-TaS$_2$ upon cooling (blue arrows) and warming the sample (red arrows), where open circles and triangles correspond to the C-CDW-like and IC-CDW-like components of the NC-CDW phase, respectively. Closed circles and triangle correspond to the C-CDW and IC-CDW phases at a temperature below the NC- to C-CDW and above the IC- to NC-CDW phase transitions, respectively. Stack of three Ta–S layers in the IC-CDW (c) and C-CDW phases (d). The atomic planes of S atoms are near straight in the former and undulating in the latter. That is because S atoms above SDs and those between SDs tend to move outward and toward Ta planes in the C-CDW phase, respectively. Thus, the displacements of S atoms in adjacent layers appear to undulate out-of-phase, where the period of the undulation is essentially the lattice parameter $\boldsymbol{a} = \sqrt{13}a_o$ of the superstructure of SDs shown in figure 1(c).

distances and show similar but near out-of-phase oscillations at distances longer than 60Å. The observation indicates that the C- to NC-CDW phase transition exhibits significant thermal hysteresis effects that largely involve longer-range atomic correlations between discommensurate domains.

4. Discussion

Evolution of Ta–Ta near neighbor distances in 1T-TaS$_2$ with temperature, as computed from the respective PDF-refined structure models, is presented in figure 5(a). As can be seen in the figure, at 400 K, i.e. in the IC-CDW phase, Ta atoms exhibit a broad distribution of near-neighbor distances indicating that they are significantly displaced from their positions in normal 1T-TaS$_2$. The distances become more distinct and characteristic to SDs with diminishing temperature. Evolution of interlayer distances in 1T-TaS$_2$ with temperature, also computed from the respective PDF-refined structure models, is shown in figure 5(b). Three-layer fragments from the IC-CDW and C-CDW models are shown in figures 5(c) and (d), respectively. The fragments are obtained by folding large-scale (∼150 Å × 150 Å × 150 Å) model configurations refined against PDF data sets obtained, respectively, at 400 K and 140 K into smaller 30 Å × 30 Å × 30 Å atomic configurations,

where the large-scale configurations are obtained by reverse Monte Carlo simulations described in supplemental material [12]. As such, the fragments provide a statistically more representative picture of the arrangement of Ta–S layers in the metallic IC-CDW (figure 4(c) to become 5(c)) and insulating C-CDW (figure 4(d) to become 5(d)) phases of 1T-TaS$_2$ than a single unit cell model would do.

As data in figures 5(b) and (c) show, layers in IC-CDW 1T-TaS$_2$, where Ta atoms exhibit signatures of clustering leading to an asymmetric broadening of first neighbor Ta–Ta distances (figure 5(a)), are straight and, at 400 K, positioned about 5.9 Å apart. As data in figures 5(b) and (d) show, layers in C-CDW 1T-TaS$_2$, where Ta atoms are clustered in well-defined SDs leading to splitting of first neighbor Ta–Ta distances into three distinct components (figure 5(a)), are undulating and, at 140 K, positioned about 5.93 Å apart. The undulation largely involves sulfur planes enclosing the array of SDs in Ta planes and shows a period of repetition of about 12 Å, which is close to the C-CDW wavelength observed by scanning tunneling microscopy [10, 24]. It is then plausible to associate the metallic state exhibited by the IC-CDW phase and IC-CDW-phase-like regions in the NC-CDW phase with the relatively closely packed, straight Ta–S layers shown in figure 5(c) wherein the SDs do not form a well-defined superstructure [27]. Then, the less closely packed, undulating
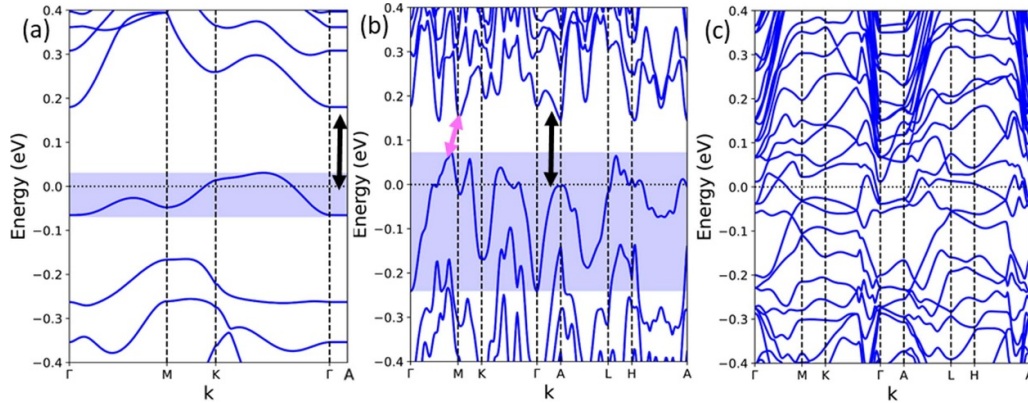
Figure 6. DFT band structure for a C-CDW monolayer (a), bulk C-CDW (b) and bulk IC-CDW 1T-TaS$_2$ (c). The band structure for the monolayer features a relatively narrow band at the Fermi level and a band gap at the zone boundary A point in the order of 0.18 eV (black arrow), which is in line with the findings of ARPES studies [24]. The band gap is seen to shrink in bulk C-CDW due to interlayer coupling. States above Fermi level could appear populated at high-temperature and empty below 180 K [27], due to diminished temperature and orbital overlap, contributing to the insulating state of C-CDW phase [26, 30]. A small indirect band gap of 0.08 eV in bulk C-CDW is indicated with a magenta arrow. Bulk IC-CDW shows metallic properties. Blue shaded rectangles in (a) and (b) highlight the valence band of monolayer and bulk C-CDW 1T-TaS$_2$.

Ta–S layers in figure 5(d), where, by contrast, the SDs form a well-defined superstructure, appear a good approximation to the atomic structure of the insulating C-CDW phase and C-CDW-phase-like domains in the NC-CDW phase of 1T-TaS$_2$. As can be seen in figure 5(b), the interlayer separations in the two fractions of the NC-CDW phase increasingly diverge upon cooling the sample from 350 K down to 180 K, inevitably leading to accumulation of significant lattice strain [10, 25]. The NC- to C-CDW phase transition is seen to involve a sudden increase in the interlayer separation in the two fractions of the NC-CDW phase by, respectively, 0.5%–1% (figure 4(b)), which would relieve the accumulated lattice strain, and not a decrease in that separation, as suggested in [28]. Importantly, the transition does not seem to involve a dramatic change in the layer stacking order, which largely retains its character on both sides of the transition (see figure S3 and the successful fits to the PDFs for the NC- and C-CDW phases in figure 4 based on the same model approximation).

This model picture helps understand the response of the C-CDW phase of 1T-TaS$_2$ to external stimuli. In particular, upon warming, the less dense in terms of layer stacking C-CDW phase may remain stable to a higher temperature (red lines in figure 5(b)) in comparison to the temperature at which it emerged from the denser in terms of layer stacking NC-CDW phase on cooling (black lines in figure 4(b)), resulting in pronounced hysteresis effects (figures 4(m) and (n)). Depending on the rate of warming induced by increasing temperature or the intensity of short laser pulses, various mixtures of the distinct layer structures seen in figures 5(c) and (d) can emerge. In this sense, the mixtures may be viewed at as a trivial outcome of the particular thermal or optical treatment conditions and not as some 'hidden' CDW phases. When high pressure is applied, Ta–S layers in the insulating C-CDW phase would be forced to come closer together, which would inevitably lead to a destruction of their undulation and related superstructure of SDs and, hence, restoration of the metallic state [4].

5. Conclusion

The lack of 3D periodicity and significant lattice distortions inherent to CDW phases often makes it difficult to describe them in terms of small size 3D periodic unit cells needed for physical properties calculations and interpretation. Therefore, 3D periodic approximations to the actual crystal structure of the phases are often considered based on plausible assumptions. Unfortunately, the approximations are not necessarily tested and refined against experimental data sensitive both to local lattice distortions and their ordering over long-range distances that are characteristic to the CDW phase being studied, posing limits to their applicability. The problem can be alleviated by using atomic PDF analysis, which takes into account all components of experimental diffraction data and, therefore, is sensitive to all structural features of CDWs, be they 3D periodic or not. The approach allows us to discriminate between competing approximations, created by e.g. reducing superspace models, DFT computations and/or educated guessing, providing a sound basis for first-principles calculations.

In particular, first-principles calculations using an approximation featuring a T_A-type stacking sequence suggest that the C-CDW phase of 1T-TaS$_2$ is a trivial band insulator and the emergence of that sequence during the NC- to C-CDW phase transition is responsible for its metal-to-insulator character [22, 26]. On the other hand, atomic PDF analysis conducted here finds that an approximation with a similar level of complexity, i.e. a minimum number of Ta–S layers in the unit cell, featuring a T_C-type stacking is superior to the T_A-type stacking sequence approximation to the structure of C-CDW phase. Therefore, we argue that the former should not be abandoned in favor of the latter but given full consideration in calculating and interpreting electronic properties. Results from DFT + U calculations for the electronic band structure of a C-CDW monolayer and bulk C-CDW phase computed from the PDF-refined approximation featuring a T_C-type stacking sequence (table S3) are shown in figure 6. The band structure

of bulk IC-CDW is also shown as computed from the PDF-refined structure data in table S1. Details of the calculations are given as supplemental material [12]. In line with the findings of prior experimental and DFT studies [26, 29–31], the electronic band structure of a C-CDW monolayer is seen to exhibit a narrow band at the Fermi level. The band has a weak in-plane dispersion (Γ–M–K–Γ line), likely due to a weak in-plane SD hybridization [26], which is consistent with the agreed Mott insulating character of the monolayer [27]. The in-plane dispersion increases and the direct band gap at the zone boundary A point (Γ–A line) narrows in bulk C-CDW 1T-TaS$_2$, indicating that the coupling between T_C-type stacked layers weakens the Mott behavior. Given the lack of a significant energy-momentum dispersion along the *c* axis (Γ–A line), it may be concluded that bulk C-CDW 1T-TaS$_2$ is neither trivial band insulator nor metallic in the layer stacking direction but largely preserves the Mott insulating state of individual layers. Then, from a structural point of view, the emergence of an insulating state upon cooling may be associated with the concurrent disappearance of the metallic IC-CDW component of the NC-CDW phase and the emergence of a 3D superstructure of SDs preexisting in the increasingly insulating C-CDW component of the NC-CDW phase with decreasing temperature, accompanied by a relief of lattice strain and not necessarily a dramatic change in the layer stacking order. Indeed, recent fully self-consistent DFT calculations also indicate that the Mott insulating nature of the C-CDW phase is independent of the stacking order [30]. The result underlines the importance of using precise crystal structure approximations in determining the nature of CDW phases. Other complex electronic phases from the TMD family, and beyond, could benefit from studies involving the experimental approach adopted here.

Data availability statement

The data that support the findings of this study are available upon reasonable request from the authors.

Acknowledgments

ORCID iDs

V Petkov https://orcid.org/0000-0002-6392-7589
J E Peralta https://orcid.org/0000-0003-2849-8472

References

[1] Rossnagel K 2011 On the origin of charge density waves in selected layered transition metal dichalcogenides *J. Phys.: Condens. Matter* **23** 213001

[2] Han T-R T, Zhou F, Malliakas C D, Duxbury P M, Mahanti S D, Kanatzidis M G and Ruan C-Y 2015 Exploration of metastability and hidden phases in correlated electron crystals visualized by femtosecond optical doping and electron crystallography *Sci. Adv.* **1** e1400173

[3] Kratochvilova M, Hillier A D, Wildes A R, Wang L, Cheong S-W and Park J-G 2017 The low-temperature highly correlated quantum phase in the charge-density-wave 1T-TaS$_2$ compounda *npj Quant. Mater.* **2** 42

[4] Sipos B, Kusmatseva A F, Akrap A, Berger H, Forro L and Tutis E 2008 From Mott state to superconductivity in 1T-TaS$_2$ *Nat. Mater.* **7** 960

[5] Xu P, Piatek J O, Lin P-H, Sipos B, Berger H, Forró L, Rønnow H M and Grioni M 2010 Superconducting phase in the layered dichalcogenide 1T-TaS$_2$ upon inhibition of the metal-insulator transition *Phys. Rev.* B **81** 172503

[6] Wang Y D, Yao W L, Xin Z M, Han T T, Wang Z G, Chen L, Cai C, Li Y and Zhang Y 2019 Band insulator to Mott insulator transition in 1T-TaS$_2$ *Nat. Commun.* **11** 4215

[7] Lee S-H, Goh J S and Gho D 2019 Origin of the insulating phase and first-order metal-insulator transition in 1T−TaS$_2$ *Phys. Rev. Lett.* **122** 106404

[8] Butler C J, Yoshida M, Hanaguri T and Iwasa Y 2020 Mottness versus unit-cell doubling as the driver of the insulating state in 1T-TaS$_2$ *Nat. Commun.* **11** 2477

[9] 2Dsemiconductors (available at: www.2dsemiconductors. com/tas2/)

[10] Thomson R E, Burk B, Zettl A and Clarke J 1994 Scanning tunneling microscopy of the charge-density-wave structure in 1*T*-TaS$_2$ *Phys. Rev.* B **49** 16899

[11] Sppijkerman A, de Boer J L, Meetsma A, Wiegers G A and van Smaalen A 1997 X-ray crystal-structure refinement of the nearly commensurate phase of 1T-TaS$_2$ in (3+2)-dimensional superspace *Phys. Rev.* B **56** 13757

[12] Supplemental material

[13] Toby B H and Von Dreele R B 2013 GSAS-II: the genesis of a modern open-source all purpose crystallography software package *J. App. Cryst.* **46** 544

[14] Kim H J, Malliakas C D, Tomić A T, Tessmer S H, Kanatzidis M G and Billinge S J L 2006 Local atomic structure and discommensurations in the charge density wave of CeTe$_3$ *Phys. Rev. Lett.* **96** 226401

[15] Petkov V, Chapagain K, Shastri S and Ren Y 2020 Genesis of the periodic lattice distortions in the charge density wave state of 2H-TaSe$_2$ *Phys. Rev.* B **101** 121114(R)

[16] Brouwer R 1978 *Doc. Thesis* University of Groningen, The Netherlands p 10459789 (available at: https://inis. iaea.org/search/search.aspx?orig_q=RN:)

[17] Walker M B and Withers R L 1983 Stacking of charge-density waves in 1T transition-metal dichalcogenides *Phys. Rev.* B **28** 2766

[18] Stahl Q, Kusch M, Heinsch F, Garbarino G, Kretzschmar N, Hanff K, Rossnagel K, Geck J and Ritschel T 2020 Collapse of layer dimerization in the photo-induced hidden state of 1T-TaS$_2$ *Nat. Commun.* **11** 1247

[19] Tanda S, Sambongi T, Tani T and Tanaka S 1984 X-ray study of charge density wave structure in 1T-TaS$_2$ *J. Phys. Soc. Japan* **53** 476

[20] Wiegers G A, de Boer J L, Meetsma A and van Smaalen S 2001 The Peierls transition in low- dimensional electronic crystals *Z. Kristallogr.* **216** 45

[21] Farrow C L, Juhás P, Liu J, Bryndin D, Bozin E S, Bloch J, Proffen T and Billinge S J L 2007 PDFfit2 and PDFgui: computer programs for studying nanostructure in crystals *J. Phys.: Condens. Matter* **19** 335219

[22] Ritschel T, Berger H and Geck J 2018 Stacking-driven gap formation in layered $1T$-TaS_2 *Phys. Rev.* B **98** 195134

[23] Ritschel T, Trinckauf J, Koepernik K, Büchner B, Zimmermann M V, Berger H, Joe Y I, Abbamonte P and Geck J 2015 Orbital textures and charge density waves in transition metal dichalcogenides *Nat. Phys.* **11** 328

[24] Hovden R *et al* 2016 Atomic lattice disorder in charge-density-wave phases of exfoliated dichalcogenides ($1T$-TaS_2) *Proc. Natl Acad. Sci.* **113** 11420

[25] Scruby C B, Williams P M and Parry G S 1975 The role of charge density waves in structural transformations of 1T TaS_2 *Phil. Mag.* **31** 255

[26] Martino E *et al* 2020 Preferential out-of-plane conduction and quasi-one dimensional electronic states in layered $1T$-TaS_2 *npj 2D Mater. Appl.* **4** 7

[27] Chen Y *et al* 2020 Strong correlations and orbital texture in single-layer $1T$-$TaSe_2$ *Nat. Phys.* **16** 218

[28] Wang W, Dietzel D and Schirmeisen A 2019 Lattice discontinuities of $1T$-TaS_2 across first order charge density wave phase transitions *Sci. Rep.* **9** 7066

[29] Yu X-L, Liu D Y, Wu J, Lin H-Q, Chang K and Zou L-J 2017 Electronic correlation effects and orbital density wave in the layered compound $1T$-TaS_2 *Phys. Rev.* B **96** 125138

[30] Shin D, Tancogne-Dejean N, Zhang J, Okyay M S, Rubio A and Park N 2021 Identification of the mott insulating charge density wave state in $1T$-TaS_2 *Phys. Rev. Lett.* **126** 196406

[31] Miller D C, Mahanti S D and Duxbury P M 2018 Charge density wave states in tantalum dichalcogenides *Phys. Rev.* B **97** 045133